Quantitative determination of the adsorption site of the OH radicals in the H_2O/Si(100) system

S. Bengió,[1] H. Ascolani,[1] N. Franco,[2,3] J. Avila,[2,3] M. C. Asensio,[2,3] E. Dudzik,[4] I. T. McGovern,[4] T. Giessel,[5] R. Lindsay,[5] A. M. Bradshaw,[5] and D. P. Woodruff[6,*]

[1]*CONICET and Centro Atómico Bariloche, Comisión Nacional de Energía Atómica, 8400 Bariloche, Argentina*

[2]*Instituto de Ciencia de Materiales, CSIC, Cantoblanco, 28049 Madrid, Spain*

[3]*LURE, Bâtiment 209D, Université Paris-Sud, F91405 Orsay, France*

[4]*Physics Department, Trinity College, Dublin 2, Ireland*

[5]*Fritz-Haber-Institut der Max-Planck-Gesellschaft, Faradayweg 4-6, 14195 Berlin, Germany*

[6]*Physics Department, University of Warwick, Coventry CV4 7AL, United Kingdom*

(Received 12 July 2002; published 26 November 2002)

Using scanned-energy mode photoelectron diffraction from the O 1*s* level, the local structure around the adsorbed OH species resulting from the interaction of H_2O with a Si(100)(2×1) has been determined, by a combination of direct data inversion using a ''projection'' method and multiple-scattering simulations. The O atom is bonded to a surface Si atom with a Si-O bond length of 1.67 ± 0.03 Å, the Si-O bond being tilted away from the surface normal by $19\pm4°$. This bonding Si atom is at one end of a surface dimer, which lies parallel to the surface to within $\pm9°$, but there appears to be a lateral offset of the dimer along the dimer direction away from the fully symmetric position by approximately 0.3 Å, possibly reflecting a residual asymmetry associated with the adsorbate bonding. The main structural parameters are in excellent agreement with the results of a previously published density-functional theory slab calculation.

DOI: 10.1103/PhysRevB.66.195322 PACS number(s): 68.43.−h, 82.45.Jn, 61.14.Qp

I. INTRODUCTION

There have been extensive ultrahigh vacuum surface science studies of the interaction of water with the Si(100) surface,[1–14] motivated by the importance of wet oxidation processes to the silicon-based industry. The clean surface of Si(100) is known to comprise (asymmetric) Si dimers to reduce the number of dangling bonds, leading to a (2×1) periodicity. Experimental studies of this system using high-resolution electron energy-loss spectroscopy[2] and infrared-absorption spectroscopy[3] have shown that the interaction of water with this Si(100)(2×1) surface below 500 K causes dissociation of the molecules and the formation of Si-H and Si-OH species. In addition, real-space information obtained by scanning-tunneling microscopy and by the technique of time-of-flight scattering and recoil spectrometry suggests that the H and OH fragments adsorb at the opposite ends of the silicon dimers, such that they saturate the remaining dangling bonds of the (2×1) surface.[7–9] On the basis of these experimental results the adsorption process of H_2O molecules on Si(100)(2×1) surfaces is considered to be understood qualitatively. However, apart from a preliminary report relating to the present study,[13] there is no quantitative information about the local adsorption structure of this system.

In this paper we present the results of a quantitative determination of the structure of the Si(100)(2×1)/H_2O surface using scanned-energy mode photoelectron diffraction (PhD).[15] This technique involves the measurement of the intensity of photoelectron emission from a core level of an adsorbate atom as a function of the incident photon energy for different emission directions. These photoelectron intensity-energy spectra show modulations caused by the coherent interference of the directly emitted component of the photoelectron wave field with components of the same wave field elastically scattered by the surrounding atoms; as the photoelectron energy, and thus the photoelectron wavelength, changes, individual scattering paths switch in and out of phase, so the observed modulations are directly related to the positions of the near-neighbor atoms relative to the emitter. In the present study, the intensity of the O 1*s* photoemission peak as a function of the photon energy was measured in nine inequivalent emission directions. These data have been analyzed to establish the local adsorption geometry of the (bonding) oxygen atoms of the OH radicals on the Si(100)(2×1) surface, using a combination of a model-free direct-inversion method followed by more quantitative analysis using multiple-scattering cluster simulations to establish the structural parameter values giving the best fit to the experimental PhD modulation curves.

II. EXPERIMENTAL DETAILS AND RESULTS

The experiments were carried out at the BESSY I synchrotron-radiation facility in Berlin using the HE-TGM 1 beam line.[16] The surface science end-station chamber is equipped with the usual sample handling and surface characterization facilities and a concentric spherical-sector electron spectrometer (VG Scientific, 152-mm radius, three channeltron detection) for recording soft-x-ray photoelectron spectroscopy (SXPS) data (including those used in the photoelectron-diffraction measurements). The Si(100) *p*-doped samples were degassed for several hours at 1000 K using resistive heating and were then flashed at 1500 K. SXPS and low-energy electron diffraction (LEED) indicated that a clean and well-ordered two-domain (2×1) reconstructed surface was obtained following this procedure. The surface was then exposed to 1×10^{-8} mbar of deionized water for 100 s at room temperature, the sharp two-domain

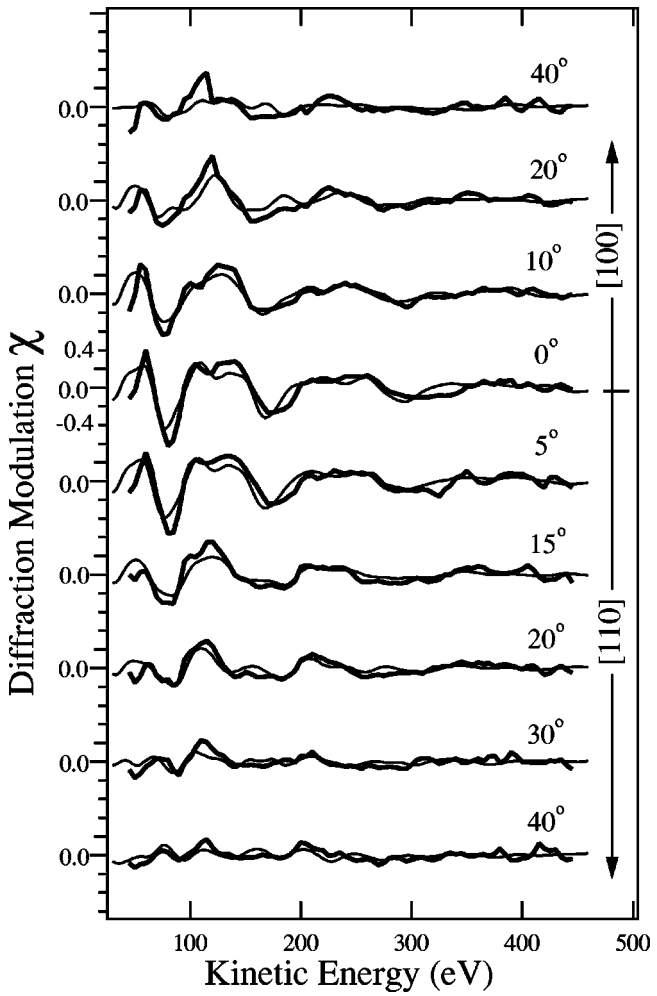

FIG. 1. Experimental O 1*s* PhD spectra from the Si(100)(2×1)/H_2O surface, recorded in the [100] and [110] azimuths at different polar emission angles relative to the surface normal, compared with the results of the best-fit multiple-scattering calculations.

(2×1) LEED pattern remained unchanged after the exposure, as reported in the literature, but SXPS clearly showed the appearance of an oxygen-containing adsorbate.

Photoelectron-diffraction data using the O 1*s* photoemission peak were recorded from this Si(100)(2×1)/H_2O surface in the kinetic-energy range 50–450 eV at polar emission angles of 0°, 5°, 15°, 20°, 30°, and 40° in the ⟨110⟩ azimuth, and at 10°, 20°, and 40° in the ⟨010⟩ azimuth. These measurements were carried out on samples cooled to 200 K in order to reduce the influence of thermal vibrations in the PhD data. For each emission direction individual photoelectron energy distribution curves (EDC's) were recorded in a 50-eV range centered on the O 1*s* emission peak at a succession of photon energies (in 5-eV increments) to cover the necessary kinetic-energy range. Each of these EDC's was fitted by a sum of a Gaussian peak with its associated background step and a suitable underlying background and the resulting peak areas as a function of photoelectron energy were normalized to a smooth spline through the data to give individual photoelectron-diffraction modulation spectra. These PhD modulation spectra (Fig. 1) are the basis of the subsequent structure determination described in the following section.

III. DATA ANALYSIS AND STRUCTURE DETERMINATION

A. Direct inversion of the experimental data

While a fully quantitative structure determination from PhD data is only possible by comparison of the experimental data with the results of computational simulations that take proper account of the effects of multiple elastic electron scattering, valuable insight into the correct structural model can often be obtained through the use of methods of direct inversion of the experimental spectra to produce a real-space ''image'' of the structure. All such inversion procedures are based on simplifications which are not strictly valid, but they can still provide valuable first indications of the probable adsorption site. In the present case we have used variations of the so-called ''projection method'' [17,18] of direct data inversion. This method is based on the fact that if the emission direction is aligned with the internuclear axis between the emitter atom and one of its substrate nearest neighbors such that the scattering is through 180°, the PhD modulations are commonly (but not invariably[19]) dominated by the interference between the directly emitted component of the photoelectron wave field and the single-scattering wave generated by the backscattering at this nearest neighbor. Simple Fourier transforms of the PhD spectra can often identify this backscattering spectrum,[20,21] and thus locate the near-neighbor direction, but this transform takes no account of the effects of the phase shifts suffered in the atomic scattering and so cannot identify the neighbor distance. Replacing the Fourier transform by a projection onto a single-scattering modulation function which takes proper account of the scattering phase shifts, however, can greatly improve this situation.

The mathematical algorithm for the projection method is as follows: first, projection coefficients for the jth measured PhD spectrum obtained in an emission direction specified by the polar and azimuthal emission angles θ_j and ϕ_j are defined as

$$c(\theta_j,\phi_j,\mathbf{r}) = r\int_{k_{\min}}^{k_{\max}} \chi_{\exp}(k,\theta_j,\phi_j)\chi_{\text{theo}}(k,\theta_j,\phi_j,\mathbf{r})dk,$$

where $\chi_{\text{theo}}(k,\theta_j,\phi_j,\mathbf{r})$ is the modulation function calculated for the emitter and a single substrate atom located at the position $\mathbf{r}$ relative to the emitter. Then, the individual projection coefficients $c(\theta_j,\phi_j,\mathbf{r})$ obtained from the different PhD spectra are combined in order to obtain a projection coefficient for the full data set. Hofmann *et al.*[17,18] defined the total projection coefficient C as

$$C(\mathbf{r}) = \sum_{j=1}^{N} s\,\exp(c(\theta_j,\phi_j,\mathbf{r})),$$

where s is an arbitrary scaling factor added in more recent implementations to adjust the ''contrast'' of the ''image'' defined by $C(\mathbf{r})$. The exponential weighting in this expression was chosen to allow the spectra with the strongest modulations, associated with the near-180° scattering condition, to

dominate the resulting ''image,'' although this obviously has the effect of suppressing the importance of other scatterers (but also of suppressing spurious features). An alternative definition of the total projection coefficient[22] in which individual coefficients are equally weighted (in a fashion more similar to the approach of Tong Huang, and Wei[23]) is

$$C(\mathbf{r}) = \sum_{j=1}^{N} c(\theta_j, \phi_j, \mathbf{r}).$$

Notice that in both definitions, due to the backscattering effect, when $\mathbf{r}$ coincides with the position $\mathbf{R_{NN}}$ of a nearest neighbor to the emitter, those coefficients $c(\theta_j, \phi_j, \mathbf{r})$ corresponding to emission directions nearly parallel to $\mathbf{R_{NN}}$ will be very intense, and the sum of their contributions gives rise to a strong maximum of the total projection coefficient $C(\mathbf{r})$. Consequently, the maxima of $C(\mathbf{r})$ indicate the most probable positions of the nearest neighbors of the emitter. One significant difference in the two definitions of $C(\mathbf{r})$ is that because the individual $c(\theta_j, \phi_j, \mathbf{r})$ can be both positive and negative (when the experimental and theoretical modulations are in antiphase), the second definition leads to values of $C(\mathbf{r})$ that can also be negative, whereas the exponential in the first form ensures that only positive values are seen. Mapping $\exp C(\mathbf{r})$ using the second definition can be used to overcome this problem and generates ''cleaner'' images.

In the present case, the total coefficient (in each definition) was calculated from 33 PhD modulation curves, derived from the original experimental data set (one normal emission, eight off-normal emissions) together with the extra off-normal spectra obtained by imposing the 2-mm point-group symmetry of the substrate. Note that this procedure does not assume that the surface has this same symmetry, but recognizes that the experimental data must average over all symmetrically equivalent domains such that this substrate symmetry is imposed on the data. $C(\mathbf{r})$ is a function in three-dimensional space and must be presented as two-dimensional cuts perpendicular and parallel to the surface. Such cuts, for all three representations of $C(\mathbf{r})$, are shown in Fig. 2 in the form of gray-scale maps. The upper panels show the standard exponential representation, the middle panels the result of equal weighting [leading to positive (black) and negative (white) values of $C(\mathbf{r})$], while the bottom panels show the exponential mapping of this equally weighted sum. On the left are shown cuts perpendicular to the surface in the [110] azimuth passing through the emitter located at (0, 0, 0). We chose the outward surface normal, defined as [001], as the z direction, with x then being along [110] and y along $[\bar{1}10]$. While the exact shape of the dominant dark feature associated with the most probable location of the Si nearest neighbor to the O emitter differs in the three ''images,'' in all cases it is directly below the emitter at a depth of approximately 1.62 Å. On the right-hand side of Fig. 2, cuts in the x-y plane parallel to the surface are shown at this depth below the emitter, confirming the position of the dominant feature as centered directly below the emitter. The clear implication of these projection method images is thus that the approximate

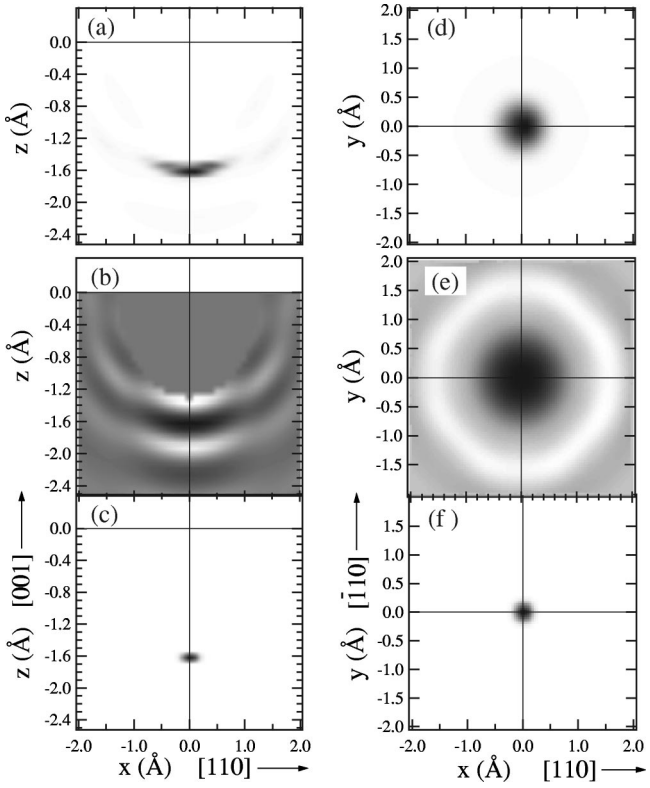

FIG. 2. Results of the application of the projection method of direct inversion of the PhD spectra of Fig. 1 to obtain approximate ''images,'' shown as gray-scale maps of $C(\mathbf{r})$, of the near-neighbor scatterer positions relative to the O emitters located at (0,0,0). Three different representations are shown. In the top two panels [(a) and (d)] the effects of the standard exponential summing definition of $C(\mathbf{r})$ (Refs. 17 and 18) are shown. In the central panels [(b) and (e)] equal weighting (Ref. 22) is used, leading to both positive (black) and negative (white) values of $C(\mathbf{r})$. At the bottom [(c) and (f)] the effects of mapping the exponential of the equally weighted $C(\mathbf{r})$ is shown. The three left-hand panels [(a)–(c)] are cuts perpendicular to the surface in the [110] azimuth, while the right-hand panels [(d)–(f)] are cuts parallel to the surface at a depth below the emitter (1.62 Å) chosen to intersect the dominant feature in the perpendicular cuts.

location of the O atom is atop a surface Si atom at a distance of approximately 1.62 Å. Notice that these images do not prove that the O atom is in the fully symmetric atop site. If the adsorption is off-atop, averaging over the symmetrically equivalent offset directions (in the experimental data as well as in our projection images) may still lead to an apparent atop site. This has been identified as a common feature of the standard projection method and is likely to be true of other direct-data-inversion methods.[19] If the true site is off-atop, a splitting of the feature in the direct method may be seen, but the significance of this effect is dependent on many aspects including the size of the data set and the nature of the atomic scattering cross section. Some systematic error in the apparent O-Si nearest-neighbor distance is also to be expected due to the effects of multiple scattering. Nevertheless, these results do provide a clear guide to the approximate structure, which may be refined by multiple-scattering simulations.

B. Quantitative determination of the atomic structure

Truly quantitative structural information must be obtained by multiple-scattering modeling of the experimental data using a succession of trial structures until an optimum fit is obtained. These calculations are performed with computational codes developed by Fritzsche, which use an expansion of the scattering processes into scattering paths.[24,25] The successive scattering events on a scattering path are treated within a Green's-function formalism using a magnetic quantum number expansion for the free-electron propagator.[26] In order to provide an objective measure of the quality of agreement between the simulated and experimental modulation functions it is important to make use of an objective criterion provided by minimization of a reliability factor (*R* factor). One such *R* factor previously used extensively in PhD structure determinations is R_m,[27] which is a normalized sum of the squares of the differences between experimental and theoretical PhD modulation amplitudes at each data point *i*, in the complete set of PhD spectra to be compared,

$$R_m = \sum_i \frac{(\chi_{\mathrm{exp}}(i) - \chi_{\mathrm{theo}}(i))^2}{(\chi_{\mathrm{exp}}(i)^2 + \chi_{\mathrm{theo}}(i)^2)}.$$

The normalization is such that R_m equals zero for complete agreement between theory and experiment, unity for no correlation between theory and experiment, and a value of 2 for anticorrelation. In the present investigation we have also explored the use of a second *R* factor R_p, in which all the χ values in the above expression are replaced by energy derivatives χ'.[28] This is rather similar to the LEED *R* factor proposed by Pendry[29] except that in the Pendry *R* factor the χ of R_m are replaced by logarithmic derivatives of the LEED intensities, I'/I. The objective in LEED was to try to match peak positions with no regard for absolute intensities. In PhD it is not possible to use the logarithmic derivative because the modulation functions pass through zero, but furthermore the actual modulation amplitudes are an important source of information which must be matched. Using simple derivatives retains a dependence on the actual amplitudes but increases the sensitivity to minor features relative to the comparison of the amplitudes alone.

In order to optimize the efficiency of the search of structural multiparameter space around trial models to find the structure corresponding to the best agreement, we use an adapted Newton-Gauss algorithm.[24] In order to define the precision of the final structural parameters, and to establish the formal significance of changes in the *R* factor between different structural models, we use a variance in the minimum value of the *R* factor, R_{min}, defined in a similar fashion to that used in conjunction with the Pendry *R* factor in LEED.[29] In particular, we take $\mathrm{var}(R_{\mathrm{min}}) = \sqrt{(2/N)} \cdot R_{\mathrm{min}}$, where *N* is the number of independent pieces of structural information contained in the data as described by us in more detail elsewhere.[30] Any structure that is found to have an associated *R* factor less than $[R_{\mathrm{min}} + \mathrm{var}(R_{\mathrm{min}})]$ is regarded as acceptable.

Figure 3 shows the basic structural model investigated in the calculations, including the definition of the associated structural parameters. The OH is bonded to a surface Si atom at one end of a dimer in an off-atop site within the [110] azimuthal plane of the dimer. Notice that the location of H atoms cannot be obtained directly from our experiment because H atoms are very weak electron scatterers and so have very little influence on PhD spectra. (Notice, of course, that as H atoms have no associated core level it is also not possible to use H as emitter atoms in a PhD study.) For this reason Fig. 3 shows neither the H atom of the adsorbed hydroxyl, nor the atomic H atom believed to be bonded to the Si atom at the other end of the surface dimer, because their locations cannot be determined by our measurements. Because PhD is dominated by the scattering from atoms that are near neighbors to the emitter, the structural parameters to which the technique is most sensitive are the distance of the O emitter to the nearest-neighbor Si atom (Si_1), d_{O1} and the angle of this interatomic direction relative to the surface normal, θ_{O1}. However, from the point of view of understanding the full structural implications of the OH adsorption, another key question is the effect that it has on the Si surface dimer. As remarked in the introduction, on the clean Si(100)(2×1) surface this dimer is asymmetric, and this asymmetry manifests itself in two ways: the Si-Si dimer bond is not parallel to the surface, and the center of this bond is offset (along the azimuth defined by the bond direction) from the symmetric position above a fourth-layer Si atom. Although there have been many experiments and theoretical (total-energy) calculations directed to determining these structural

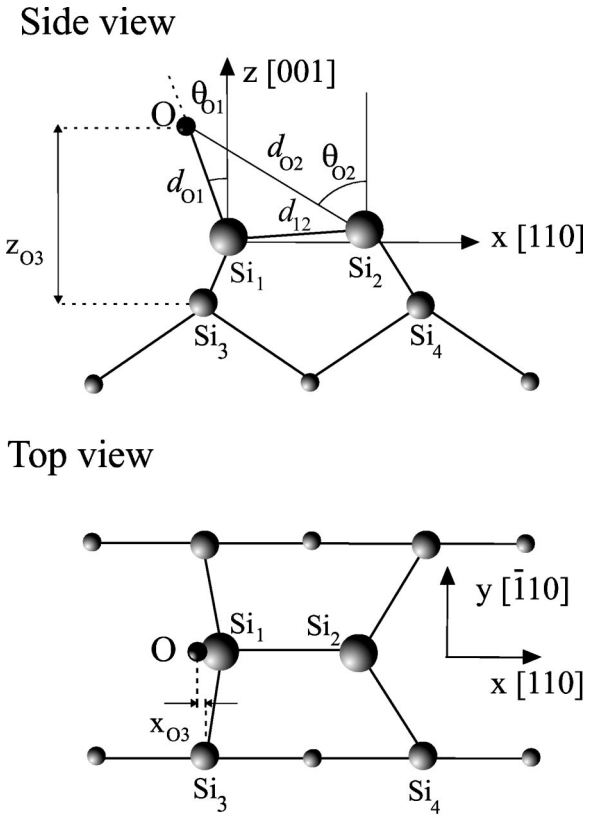

FIG. 3. Side and plan views of the local adsorption structure of OH on Si(100)(2×1) including the definition of the main structural parameters investigated in this study. The H atoms are omitted from the figure.

properties of the clean surface, the situation is complicated by the fact that the room-temperature Si(100)(2×1) structure is believed to be formally disordered with respect to the (dynamically flipping) dimer asymmetry, and while ordered asymmetric dimer phases also exist at low temperature [notably, but not only, $c(4\times2)$], these larger surface mesh structures are more difficult to study. Nevertheless, a survey of many of these studies suggests that the Si-Si dimer bond length is in the range 2.27 ± 0.02 Å, and that this bond is tilted relative to the surface plane by $17\pm3°$.[31] The lateral offset of the dimer seems to have been investigated only by theoretical calculations of the larger unit mesh truly ordered phases, which indicate a value of approximately 0.2 Å towards the ''up'' Si atom of the dimer (see, e.g., Ref. 32).

In the case of the present PhD study our data are sensitive to the location of substrate scatterer atoms relative to the O emitter, and while the greatest sensitivity is to the relative location of the nearest-neighbor Si_1 atom of Fig. 3, the other substrate atoms also contribute to the measured modulations. We assume that all the Si substrate layers below the outermost dimer layer are in a bulk-terminated structure, a situation that is quite close to that found in theoretical studies of the clean surface, and in this way we obtain information of modest precision on the location of the O atom relative to this underlying substrate (via the parameters x_{O3} and z_{O3}) and thus also of the relative position of Si_1 to this substrate. As such we gain indirect information on the dimer asymmetry through the offset of one end of the dimer. To obtain direct information on the dimer bond length and asymmetry we need to locate the Si_2 atom at the other end of the dimer, and this single scatterer atom, which is more distant from the emitter than Si_1 and in a less favorable scattering geometry, contributes only weakly to the PhD spectra and thus can only be located with much lower precision.

The best-fit structural parameter values are summarized in Table I, while the quality of the fit between theory and experiment for these values may be seen in Fig. 1. The fit is clearly rather good, as reflected by the value of R_m of 0.23; in many previous PhD structural studies that have used this R factor it has been found that values below 0.3 are generally reliable (much lower values usually being obtained only for highly symmetric surface structures, which lead to very strong modulation amplitudes). The best-fit value of R_p is 0.28, but in this case we have no similarly large body of previous applications by which to judge this value.[28] As expected, the best precision in Table I is for the nearest-neighbor Si-O bond length, d_{O1}; Fig. 4 shows R-factor contour maps of the dependence of the quality of fit on this parameter and the associated bond angle, θ_{O1}. The bold contours correspond to values of the R factors equal to the sum of the minimum value and the estimated variance; parameter values that fall within these bold contours are those that are formally judged to be within our estimated error limits. There are subtle differences in the contours for the two different R factors, and indeed there is a small difference in d_{O1} of approximately 0.02 Å in the location of the minima, which must be regarded as some estimate of a systematic error in our procedure. This value is smaller than the estimated random error.

TABLE I. Summary of the structural parameter values (Fig. 2) found in the present PhD study of Si(100)/H_2O, compared with some representative theoretical values as described in the text.

	Si(100)/H_2O (this work)	Si(100)/H_2O theory (slab[a]/cluster[b])	''Symmetric dimer'' (theory[c])
d_{O1} (Å)	1.67 ± 0.03	1.65/1.76	
θ_{O1} (°)	19 ± 4	21/26.7	
x_{O1} (Å)	-0.54 ± 0.10		
z_{O1} (Å)	1.58 ± 0.05		
d_{O2} (Å)	3.32 ± 0.14		
θ_{O2} (°)	61 ± 7		
x_{O3} (Å)	-0.18 ± 0.1		
z_{O3} (Å)	2.75 ± 0.05		
x_{13} (Å)	0.36 ± 0.15		0.80
z_{13} (Å)	1.16 ± 0.07		1.03
x_{23} (Å)	2.73 ± 0.25		3.04
z_{23} (Å)	1.13 ± 0.36		1.03
d_{12} (Å)	2.36 ± 0.30	2.38/2.46	2.24
θ_{12} (°)	1 ± 9	2/0	0

[a]Reference 35.
[b]Reference 34.
[c]Reference 33.

The much lower precision with which the location of the Si_2 atom, at the other end of the dimer, can be found is reflected in the R-factor contour maps of Fig. 5. In part this poor precision reflects the fact that none of the PhD spectra used in the analysis is close to the O-Si_2 internuclear direction corresponding to the favored 180° backscattering from this Si surface atom, although in view of the larger internuclear distance the modulations would not be expected to be very strong even in this direction. The R-factor contour maps relevant to the location of the Si_2 atom also show a significant difference in the precision estimates that are provided by the two different R factors, with R_p showing a much more localized minimum and thus substantially better precision estimates. Thus, using the appropriate R contour in R_p one finds that d_{O2} has an optimum value of 3.32 ± 0.14 Å and θ_{O2} is found to be $61\pm7°$. The error estimates for this angle using R_m are slightly larger at approximately $\pm9°$; for the interatomic distance the negative error is approximately 0.15 Å, but the contour map of Fig. 5 suggests that the positive error limit may be infinite (i.e., indicating that removing the Si_2 atom completely leaves the value of R_m within the acceptable limits). This general behavior is consistent with the idea that R_p should be more sensitive to weaker features in the PhD spectra and thus to structural parameters that have a relatively small effect on the spectra. While this raises an important question as to which error estimates should be cited (in Table I, the values derived from R_p are shown), it is important to note that the two R factors do show almost exactly the same optimum values of the related parameters, so the issue is only of precision.

A more general point concerning precision relates to the fact that because PhD is sensitive to the location of scatterer atoms relative to the emitter, more general structural parameters, such as the coordinates of the Si dimer atoms (and their

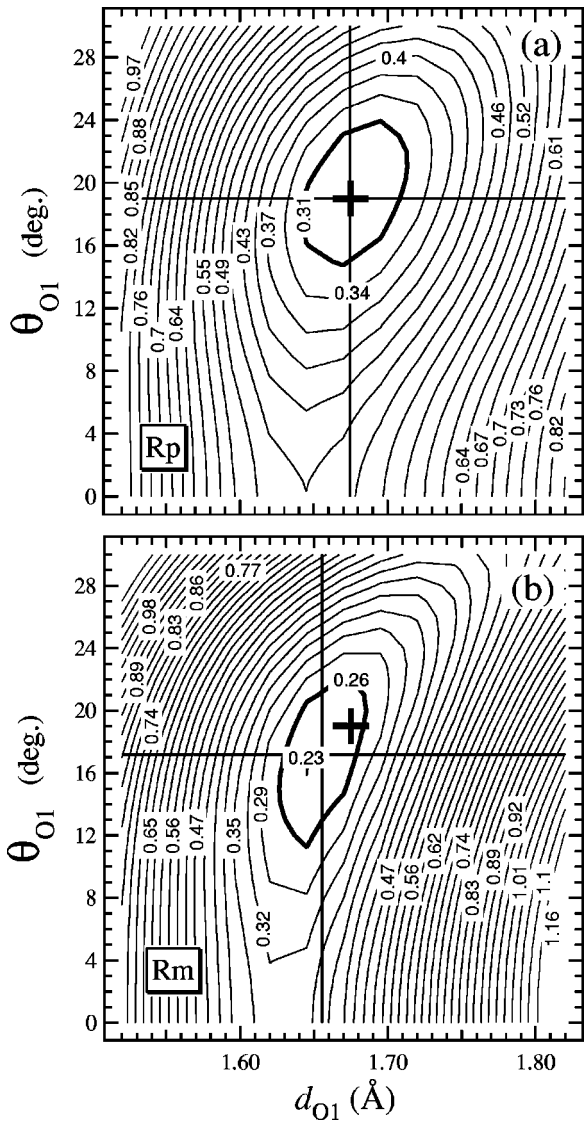

FIG. 4. *R*-factor contour maps for R_m and R_p showing the dependence of the quality of experiment-theory fit on the two primary structural parameters d_{O1} and θ_{O1}. The bold contours define the estimated precision limits.

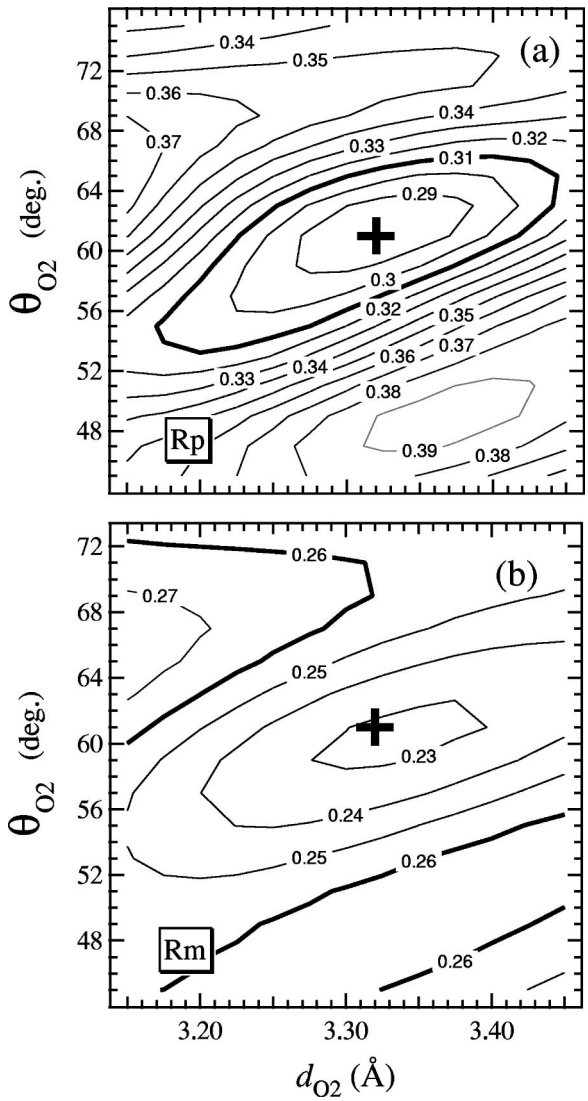

FIG. 5. *R*-factor contour maps for R_m and R_p showing the dependence of the quality of experiment-theory fit on the two structural parameters, d_{O2} and θ_{O2}, which define the location of the Si atom at the opposite end of the Si surface dimer relative to the O atom of the adsorbed OH. The bold contours define the estimated precision limits.

precision) relative to the substrate, must be deduced by simple geometry from the relevant coordinates relative to the O emitter. For this reason, the values of these ''secondary'' parameters are distinguished in Table I by being shown in italics.

IV. DISCUSSION AND CONCLUSIONS

The structural parameter values of Table I are the main conclusions of this investigation. Most clearly, these show that the O atom of the adsorbed hydroxyl species bonds to a surface Si atom with a Si-O bond length of 1.67 ± 0.03 Å, the Si-O bond being tilted away from the surface normal by $19 \pm 4°$. Our analysis actually assumes that this tilt is in the same [110] azimuthal plane as the Si dimer, but separate calculations allowing for the possibility of a twist out of plane indicate that while some modest twist is within the precision limits, no significant improvement is achieved by this. While less precise, our results also provide information on the influence of the adsorbed OH (and H) on the Si surface dimer. In particular, we find the dimer is parallel to the surface (within 9°) with a bond length of 2.36 ± 0.30 Å. The parallel orientation is indicative of a symmetric dimer, although there appears to be a significant lateral offset along the dimer direction away from the truly symmetric position of 0.3–0.4 Å. Table I includes some local coordinates calculated for a symmetric dimer on the clean Si(100)(2×1) surface.[33] While this is not actually a structure that is believed to occur in reality (the asymmetric dimer being of lower energy) it provides a useful reference for the *x* coordinates, in particular, of the Si dimer atoms Si_1 and Si_2. For a clean surface, of course, the dimer tilt and lateral offset must accompany each other, as the bond lengths between the Si

dimer atoms and those in the underlying substrate must be very similar at the two ends of the dimer. Strictly, with OH bonded to one end of the dimer and H bonded to the other, this constraint is relaxed. Our results actually imply that these bond lengths to the underlying substrate are 2.27 Å for the Si atom bonded to the OH (d_{13}) and 2.49 Å for the Si at the other end of the dimer, which is believed to be bonded to atomic H (d_{24}). Bearing in mind the limited precision of the lateral positions of the Si dimer atoms, however, the significance of these implied deviations from the bulk Si-Si bond length of 2.35 Å is difficult to assess. Of course, we should also remark that with OH and H bonded to the two ends of the Si dimer, perhaps with quite different bonding character, a truly symmetric dimer is not really to be expected. Nevertheless, the results do indicate that the Si-Si dimer orientation in the $Si(100)/H_2O$ phase is significantly more nearly parallel to the surface than on the clean surface. A somewhat similar result has been reported previously for the $Si(100)/NH_3$ system in which NH_2 and H are believed to be bonded to opposite ends of the surface dimers.[31]

Although there have been a few theoretical (total-energy) studies of this adsorption system, there appear to be only two such studies that report optimized structural parameter values; both of these are based on density-functional theory, but one involves calculations on clusters to represent the surface[34] while the other uses a slab representation.[35] The values obtained in these calculations for dimers having OH and H bonded to the two ends are also included in Table I. Comparison with the results of our experiments clearly shows excellent agreement with the results of the slab calculation, all values falling within our error estimates; while the values given by the cluster calculations are quite similar, the Si-O nearest-neighbor bond length and bond angle both fall outside the range of values given by our experiments.

In summary, our O 1*s* PhD study of the $Si(100)/H_2O$ adsorption system shows that the O atom of the resulting OH adsorbate is bonded to a Si surface atom in a near-atop site, and this Si atom is at one end of a surface dimer that is essentially parallel to the surface, although it does appear to be offset along the dimer direction away from the location which would be expected for a fully symmetric dimer on a clean Si(100) surface.

ACKNOWLEDGMENTS

This work has been partially supported by the ECOS-SECYT (Project No. A99E03) and the CSIC/CONICET (Project No. 99AR0004) collaboration programs between France and Argentina, and Spain and Argentina, respectively. The support of the European Community through the Human Capital and Mobility Networks (Grant No. ERB-CHRXCT930358) and Large-Scale Facilities programme is acknowledged. We thank V. Fritzsche for the provision of the multiple-scattering code and C. Muller and A.J. Patchett for their assistance in the original data collection.

*Corresponding author. Electronic address: d.p.woodruff@warwick.ac.uk

[1] P. Thiel and T. E. Madey, Surf. Sci. Rep. **7**, 211 (1987).
[2] H. Ibach, H. Wagner, and D. Bruchmann, Solid State Commun. **42**, 457 (1982).
[3] Y. J. Chabal and S. B. Christman, Phys. Rev. B **29**, 6974 (1984).
[4] C. U. S. Larsson, A. S. Flodstrom, R. Nyholm, L. Incoccia, and F. Senf, J. Vac. Sci. Technol. A **5**, 3321 (1987).
[5] C. U. S. Larsson, A. L. Johnson, A. Flodstrom, and T. E. Madey, J. Vac. Sci. Technol. A **5**, 842 (1987).
[6] C. Poncey, F. Rochet, G. Dufour, H. Roulet, F. Sirotti, and G. Panaccione, Surf. Sci. **338**, 143 (1995).
[7] L. Andersohn and U. Köhler, Surf. Sci. **284**, 77 (1993).
[8] M. Chander, Y. Z. Li, J. C. Patrin, and J. H. Weaver, Phys. Rev. B **48**, 2493 (1993).
[9] J. Bu and J. W. Rabalais, Surf. Sci. **301**, 285 (1994).
[10] N. Russo, M. Toscano, V. Barone, and F. Lelf, Surf. Sci. **180**, 599 (1987).
[11] S. Katircioglu, Surf. Sci. **187**, 569 (1987).
[12] C. K. Ong, Solid State Commun. **72**, 1141 (1989).
[13] N. Franco, J. Chrost, J. Avila, M. C. Asensio, C. Müller, E. Dudzik, A. J. Patchett, I. T. McGovern, T. Gießel, R. Lindsay, V. Fritzsche, A. M. Bradshaw, and D. P. Woodruff, Appl. Surf. Sci. **123/124**, 219 (1998).
[14] Y. Okamoto, Phys. Rev. B **60**, 10 632 (1999).
[15] D. P. Woodruff and A. M. Bradshaw, Rep. Prog. Phys. **57**, 1029 (1994).
[16] E. Dietz, W. Braun, A. M. Bradshaw, and R. L. Johnson, Nucl. Instrum. Methods Phys. Res. A **239**, 359 (1985).
[17] Ph. Hofmann and K.-M. Schindler, Phys. Rev. B **47**, 13 941 (1993).
[18] Ph. Hofmann, K-M. Schindler, S. Bao, A. M. Bradshaw, and D. P. Woodruff, Nature (London) **368**, 131 (1994).
[19] D. P. Woodruff, P. Baumgärtel, J. T. Hoeft, M. Kittel, and M. Polcik, J. Phys.: Condens. Matter **13**, 10 625 (2001).
[20] V. Fritzsche and D. P. Woodruff, Phys. Rev. B **46**, 16 128 (1992).
[21] K.-M. Schindler, Ph. Hofmann, V. Fritzsche, S. Bao, S. Kulkarni, A. M. Bradshaw, and D. P. Woodruff, Phys. Rev. Lett. **71**, 2054 (1993).
[22] H. Ascolani, J. Avila, N. Franco, and M. C. Asensio, Phys. Rev. Lett. **8**, 2604 (1997).
[23] S. Y. Tong, H. Huang, and C. M. Wei, Phys. Rev. B **46**, 2452 (1992).
[24] V. Fritzsche, Surf. Sci. **213**, 648 (1989).
[25] V. Fritzsche, J. Phys.: Condens. Matter **2**, 1413 (1990).
[26] V. Fritzsche, Surf. Sci. **265**, 187 (1992).
[27] R. Dippel, K.-U. Weiss, K-M. Schindler, P. Gardner, V. Fritzsche, A. M. Bradshaw, M. C. Asensio, X. M. Hu, D. P. Woodruff, and A. R. González-Elipe, Chem. Phys. Lett. **199**, 625 (1992).
[28] S. Bengió, M. Martin, J. Avila, M. C. Asensio, and H. Ascolani, Phys. Rev. B **65**, 205326 (2002).
[29] J. B. Pendry, J. Phys. C **12**, 937 (1980).
[30] N. A. Booth, R. Davis, R. Toomes, D. P. Woodruff, C. Hirschmugl, K.-M. Schindler, O. Schaff, V. Fernandez, A. Theobald, Ph. Hofmann, R. Lindsay, T. Gießel, P. Baumgärtel, and A. M. Bradshaw, Surf. Sci. **387**, 152 (1997).

[31] N. Franco, J. Avila, M. E. Davila, M. C. Asensio, D. P. Woodruff, O. Schaff, V. Fernandez, K.-M. Schindler, V. Fritzsche, and A. M. Bradshaw, J. Phys.: Condens. Matter **9**, 8419 (1997).
[32] J. E. Northrup, Phys. Rev. B **47**, 10 032 (1993).
[33] M. C. Payne, N. Roberts, R. J. Needs, M. Needels, and J. D. Joannopoulos, Surf. Sci. **211/212**, 1 (1989).
[34] R. Konečný and D. J. Doren, J. Chem. Phys. **106**, 2426 (1997).
[35] A. Vittadini, A. Selloni, and M. Casarin, Phys. Rev. B **52**, 5885 (1995).